Structural transformation in densified silica glass: A molecular-dynamics study

Wei Jin, Rajiv K. Kalia, and Priya Vashishta
Concurrent Computing Laboratory for Materials Simulations, Department of Physics & Astronomy and Department of Computer Sciences, Louisiana State University, Baton Rouge, Louisiana 70803-4001

José P. Rino
Universidade Federal de São Carlos, 13560 São Carlos, São Paulo, Brazil
(Received 11 June 1993; revised manuscript received 21 January 1994)

Pressure-induced structural transformation and the concomitant loss of intermediate-range order (IRO) in high-density SiO_2 glass are investigated with the molecular-dynamics (MD) approach. The MD simulations cover a wide range of mass densities—from normal density (2.20 g/cm^3) to the density corresponding to stishovite (4.28 g/cm^3). This twofold increase in the density produces significant changes in the short-range order and intermediate-range order. As the density increases from 2.20 to 4.28 g/cm^3, the Si-O bond length increases from 1.61 to 1.67 Å, the Si-O and O-O coordinations change from 4 to 5.8 and from 6 to 12, respectively, and the O-Si-O bond angle changes from 109° to 90°. These results provide firm evidence of structural transition from a corner-sharing $Si(O_{1/2})_4$ tetrahedral network to a network of $Si(O_{1/3})_6$ octahedra jointed at corners and edges. At normal density, the first sharp diffraction peak (FSDP) in the static structure factor $S(q)$ is at 1.6 Å^{-1} whereas under pressure the height of the FSDP is considerably diminished and its position shifts to larger q values. At a density of 2.64 g/cm^3, a peak in $S(q)$ appears at 2.85 Å^{-1}. The height of this peak grows as the density increases. All of these results are in agreement with the recent high-pressure x-ray measurements on SiO_2 glass.

I. INTRODUCTION

In recent years, silica and germania under high pressures have been studied extensively.[1–24] Silica is particularly interesting because of its many polymorphs.[25–33] Only a few of these polymorph structures are thermodynamically stable: β-cristobalite (cubic),[29] α-quartz (trigonal),[30] and β-quantz (hexagonal)[26] are stable at normal pressure whereas coesite (monoclinic)[32] and stishovite (tetragonal)[33] are stable at high pressures. The lowest-density crystalline structure, β-cristobalite is cubic at a mass density of 2.20 g/cm^3. Stishovite, the densest crystalline structure (mass density of 4.28 g/cm^3), has tetragonal symmetry.[33] Except stishovite, all stable phases of crystalline silica consist of $Si(O_{1/2})_4$ tetrahedral units linked at corners. Stishovite, on the other hand, has distorted $Si(O_{1/3})_6$ octahedra linked at corners and edges.[33]

Crystalline silica exhibits a number of structural transformations with varying temperature and pressures.[27] Low-temperature quartz (α-quartz) undergoes[27] a structural transformation into the high-temperature β-quartz at 846 K. At room temperature, quartz changes into coesite under pressure.[27] With further increase in pressure, coesite transforms into stishovite at 8.2 GPa. Quartz can also become amorphous at very high pressures.[14] The structural order of silica glass (a-SiO_2) can be divided into short-range order (SRO) and intermediate-range order (IRO).[31] Neutron,[34] x-ray,[35,36] and nuclear magnetic resonance (NMR)[37] experiments reveal the presence of corner-sharing $Si(O_{1/2})_4$ tetrahedra in normal-density (2.20 g/cm^3) silica glass. The intermediate-range order is manifested as the first sharp diffraction peak (FSDP) in neutron and x-ray diffraction static structure factors.[31] Occurring at 1.6 Å^{-1}, structural correlations that give rise to the FSDP are in the range of 5–10 Å.

Under high pressures (beyond 12 GPa), it is well known[38] that SiO_2 glass undergoes permanent density increase (densification) at room temperature. Recently, Brillouin,[4] Raman,[4–6] infrared,[6,7] neutron,[11], and x-ray[9] scattering techniques have been used to investigate the influence of pressure on a-SiO_2. Irreversible changes in Brillouin and Raman spectra have been observed in glass samples recovered after being subjected to a pressure of 17 GPa. Hemley *et al.*[5] measured Raman spectra of SiO_2 glass under pressure in a diamond-anvil cell. Between 8 and 30 GPa, they also find irreversible changes. Recently, Meade, Hemley, and Mao[9] have carried out *in situ* x-ray measurements of the static structure factor $S(q)$ of SiO_2 glass subjected to pressure of 8–42 GPa in a diamond-anvil cell. With increasing pressure, they have observed the following changes in the structure of SiO_2 glass. (1) The height of the FSDP decreases and its position shifts to higher values of q. Around 42 GPa, the FSDP almost disappears. (2) At a pressure of 28 GPa, a peak appears at 3.18 Å^{-1}. This peak grows with an increase in pressure. (3) The pressure has little influence on $S(q)$ at higher values of q. By inverting the static structure factor into the pair-correlation function, Meade, Hemley, and Mao[9] have found that the average nearest-neighbor coordination of Si atoms changes from 4 to 6.

In this paper, we report the results of a molecular-dynamics (MD) study of the influence of pressure on structural correlations in SiO_2 glass.[39] The simulations are based on effective interatomic potentials which consist of two-body and three-body interactions.[40] The

two-body potentials incorporate the effects of charge transfer, steric repulsion, and electronic polarizability of atoms. The three-body potentials take into account the covalent interactions. In the normal-density glass (2.20 g/cm^3), the calculated static structure factor and bond-angle distributions are in accord with neutron scattering and NMR measurements. With an increase in the density of the glass, the MD simulations reveal the gradual disappearance of the FSDP. Concomitantly, a peak in $S(q)$ appears at 2.85 Å^{-1} and this peak grows with the increase in the density. When the density reaches 4.28 g/cm^3, we observe a structural transformation in SiO_2 glass: the average coordinations of Si and O atoms increase to nearly 6 and 3, respectively. The O-Si-O bond-angle distribution develops peaks at 90° and 180° (at normal density, the peak is at 109°), while the Si-O-Si bond-angle distribution has peaks at 95° and 128°. The changes in coordinations and bond-angle distributions at this high density are manifestations of an amorphous phase of silica in which the structural units are $Si(O_{1/3})_6$ octahedra joined at corners and edges. These results are in complete agreement with the x-ray measurements of Meade, Hemley, and Mao.[9]

The outline for the remaining of this paper is as follows. In Sec. II, we provide details of the MD simulation for a-SiO_2. Results for pair distribution functions, bond-angle distribution functions, and static structure factors are discussed in Sec. III. A comparison with neutron and x-ray scattering measurements is also contained in this section. The conclusions from the MD simulation studies are discussed in Sec. IV.

II. CALCULATIONS

Molecular-dynamics simulations are carried out in a (N,Ω,E) ensemble for $N=648$ atoms (216 Si and 432 O) in a cubic box of volume $\Omega=L^3$. For the normal-density system, the length of the MD cell (L) is chosen to be 21.391 Å so that the mass density ρ_0 is 2.20 g/cm^3. We have also simulated systems with cell lengths 20.122, 19.434, 18.285, and 17.135 Å, which correspond to mass densities of 2.64, 2.94, 3.53, and 4.28 g/cm^3, respectively. Periodic boundary conditions (PBC) are used in all cases. The long-range Coulomb potential and forces are calculated with the Ewald summation technique.[41] In order to accelerate the calculation, a sufficiently large lookup table for two-body potentials and forces is used. The equations of motion are integrated with Beeman's algorithm using a time step $\Delta t=0.5\times10^{-15}$ sec. The total energy of the system is conserved to at least 1 part in 10^4 over ten thousands of MD time steps.

The simulations reported here are based on a combination of two-body and three-body effective interatomic potentials,

$$V(\{\mathbf{r}_i\})=\sum_{i<j}V_2(r_{ij})+\sum_{i<j<k}V_3(\mathbf{r}_{ij},\mathbf{r}_{jk},\mathbf{r}_{ik})\ , \tag{1}$$

where $\mathbf{r}_i$ is the position of atom i, $\mathbf{r}_{ij}=\mathbf{r}_j-\mathbf{r}_i$, and $r_{ij}=|\mathbf{r}_{ij}|$. The two-body potential is given by

$$V_2(r_{ij})=\frac{Q_iQ_j}{r_{ij}}-\frac{\frac{1}{2}(\alpha_iQ_j^2+\alpha_jQ_i^2)}{r_{ij}^4}\exp\left[-\frac{r_{ij}}{r_{4s}}\right]+A_{ij}\left[\frac{\sigma_i+\sigma_j}{r_{ij}}\right]^{\eta_{ij}}\ . \tag{2}$$

The first term is the long-range Coulomb interaction due to charge transfer between Si and O. The second term denotes the charge-dipole interaction, where α_i is the electronic polarizability of the atom i and r_{4s} is a screening length. The last term is the steric repulsion, with A_{ij} and η_{ij} being the strength and exponent of the steric repulsion between atoms i and j, and σ_i the effective radius of atom i.

In the simulations, we have included two kinds of three-body interactions, O-Si-O and Si-O-Si. In both cases, the three-body potential has the form

$$V_3(\mathbf{r}_{ij},\mathbf{r}_{jk},\mathbf{r}_{ik})=B_{jik}\exp\left[\frac{a}{r_{ij}-r_0}+\frac{a}{r_{ik}-r_0}\right]\times[\cos\theta_{jik}-\cos\bar{\theta}_{jik}]^2\times\Theta(r_0-r_{ij})\Theta(r_0-r_{ik})\ , \tag{3}$$

where B_{jik} is the strength of the three-body potential, θ_{jik} is the angle between r_{ij} and r_{ik}, and Θ is the step function. The range r_0 of three-body interactions is taken to be 2.6 Å.

Effective charges on Si and O atoms are taken to be $+1.6|e|$ and $-0.8|e|$, respectively. The exponents in the steric repulsion are chosen as $\eta_{\text{Si-Si}}=11$, $\eta_{\text{Si-O}}=9$, and $\eta_{\text{O-O}}=7$. The effective radii of Si and O atoms are $\sigma_{\text{Si}}=0.47$ Å and $\sigma_{\text{O}}=1.29$ Å. Reference 40 has a detailed description of how the parameters in V_2 and V_3 are chosen.

The SiO_2 glasses are generated by quenching well-thermalized liquids. We start with a well-equilibrated SiO_2 liquid at ~4000 K and the experimental normal glass density ($\rho=2.20$ g/cm^3). This liquid is cooled to 2500 K and thermalized for over 60 000 time steps. The cooling schedule involves velocity scaling at intervals of $10\Delta t$. The velocities of atoms are also scaled in the first half of the thermalization process to hold the system at the required temperature. Subsequently, the system is allowed to reach equilibrium without any disturbance. The thermalized liquid at 2500 K is further quenched by reducing the velocity of each atom by 0.01% at intervals of 10 time steps. At 1500 K the system undergoes thermal arrest. It is thermalized for 60 000 time steps at that temperature. With repeated quenching and thermalization, we obtain relaxed glassy states at 600, 300, and 1 K. After thermalization at each temperature, structural and dynamical properties are calculated with MD trajectories of over 60 000 time steps.

Instead of applying pressure to the glass, the high-density glassy states were prepared by simultaneously reducing the length of the MD cell and positions of all the atoms in the high-temperature (3500–6000 K) liquid states.[42] This was done because the diffusion of atoms in the liquids allows the system to relax more rapidly than

the low-temperature glass. The high-density liquids are thermalized for 60 000–120 000 time steps. Subsequently the above quenching-thermalization procedure is applied to produce well-relaxed glassy states at 1500, 600, 300, and 1 K.

The normal- and high-density glasses at 1 K were further quenched to zero temperature by removing all the kinetic energy from the system and by the conjugate-gradient minimization method.[43] The latter brings a system to a *zero-force* configuration. These zero-force configurations were used to calculate eigenvalues and eigenvectors of the vibrational normal modes.

We have also carried out MD simulation for crystalline stishovite since stishovite provides a reference structure for discussing the structure of the highest-density (4.28 g/cm^3) glass. The simulation for stishovite is performed[42] with $N=720$ atoms (240 Si and 480 O, $4\times5\times6=120$ tetragonal unit cells) in an orthorhombic MD box at the stishovite density of 4.28 g/cm^3. The edge lengths of the MD box are 16.720, 20.900, and 15.996 Å in the x, y, and z directions, respectively. The simulation was initiated by allocating the Si and O atoms into the tetragonal lattice at zero temperature, and giving each atom a small displacement at random direction relative to its lattice site. The first few thousand MD steps were run with a reduced time step of $\Delta t'=0.5\times10^{-16}$ sec. Pair distribution functions and bond-angle distribution functions were calculated. Using a time step of $\Delta t=0.5\times10^{-15}$ sec, the system was heated slowly to 300 K and thermalized for 10 000 time steps, then heated to 800 K and thermalized for 10 000 time steps. The system was heated to 1500 K and thermalized for 30 000 time steps. The 1500 K system was cooled slowly to 300 K and thermalized for 30 000 time steps. After this was done, it was run uninterruptedly for more than 30 000 time steps. Pair distribution functions and bond-angle distribution functions were calculated to ascertain the symmetry and *dynamical stability* of the system. We found the resulting final symmetry of the system to be the same as that of the starting tetragonal structure.

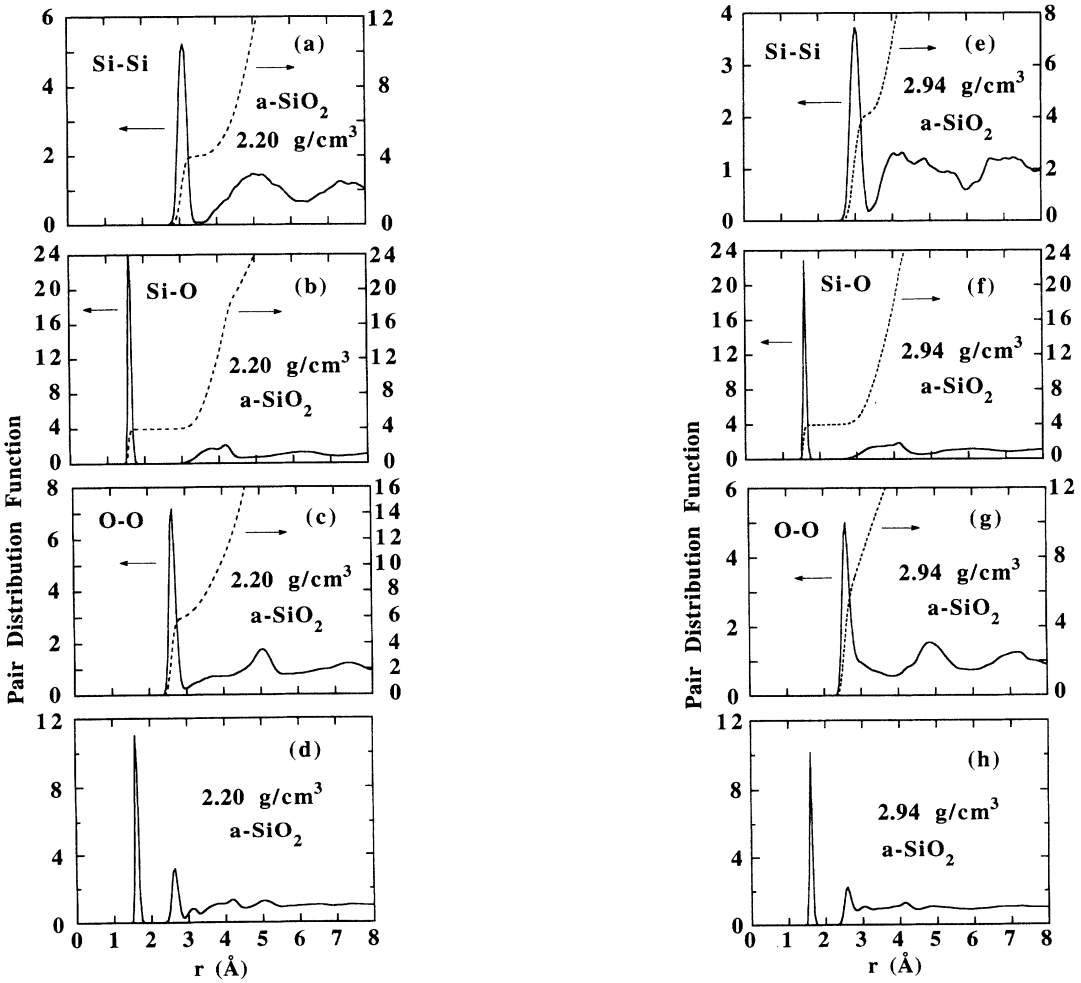

FIG. 1. Si-Si (a), (e), (i), and (m), Si-O (b), (f), (j), and (n), and O-O (c), (g), (k), and (o) partial pair distribution functions (solid lines), coordination numbers (dashed lines), and total pair distribution functions (d), (h), (l), and (p) for normal-density and high-density SiO_2 glasses at 300 K. Sharp peaks (solid lines) in the figure at 4.28 g/cm^3 (m), (n), (o), and (p) correspond to pair distribution functions for stishovite at zero temperature (the amplitudes are reduced). The dashed line in (p) corresponds to the total pair distribution function for crystalline stishovite at 300 K (the amplitude is reduced).

III. RESULTS

A. Pair distribution functions

The influence of pressure on short- and intermediate-range order is inferred from pair distribution functions, bond-angle distribution functions, static structure factors, and ring distributions. The partial pair distribution function is determined from

$$g_{\alpha\beta}(r)=\frac{\Omega\langle n_{\alpha\beta}(r,r+\Delta r)\rangle}{4\pi r^2\Delta r N_\beta}, \quad (\alpha,\beta=\mathrm{Si,O}) , \tag{4}$$

where $\langle n_{\alpha\beta}(r,r+\Delta r)\rangle$ is the average number of atoms of type β surrounding an atom of type α in a spherical shell between r and $r+\Delta r$, and N_β is the total number of atoms of type β. The total pair distribution function is obtained from

$$g(r)=\sum_\alpha\sum_\beta c_\alpha c_\beta g_{\alpha\beta}(r) , \tag{5}$$

where $c_\alpha=N_\alpha/N$ is the concentration of the α species. The average coordination number $n_{\alpha\beta}(R)$ can be calculated from

$$n_{\alpha\beta}(R)=4\pi c_\beta n\int_0^R g_{\alpha\beta}(r)r^2dr , \tag{6}$$

where $n=N/\Omega$ is the average number density.

In Fig. 1 we show the computed partial and total pair distribution functions and coordination numbers in the normal- and high-density glasses at 300 K. At the highest density, 4.28 g/cm^3, the pair distribution functions for the glass are compared with those for stishovite. In the normal-density glass, the position of the first peak in $g_{\mathrm{Si\text{-}O}}(r)$ is at 1.61 Å and there is a clear shell (plateau) of nearest-neighbor (NN) Si-O tetrahedral coordination. As the glass density increases from 2.20 to 3.53 g/cm^3, the position of the first peak in $g_{\mathrm{Si\text{-}O}}(r)$ and the corresponding Si-O coordination remain unchanged. At a pressure of 42.5 GPa, where the glass density (4.28 g/cm^3) reaches the stishovite density, the first peak in $g_{\mathrm{Si\text{-}O}}(r)$ occurs at 1.67 Å [with a full width at half maximum (FWHM) of 0.20 Å] instead of 1.61 Å and the average nearest-neighbor Si-O coordination increases from 4 to 5.8. Note that, in stishovite, the Si-O bond lengths are 1.76 and 1.81 Å and the Si-O coordination is 6. In the normal-density system, $g_{\mathrm{Si\text{-}O}}(r)$ has a gap between 1.90 and 2.98 Å and a small shoulder around 3.80

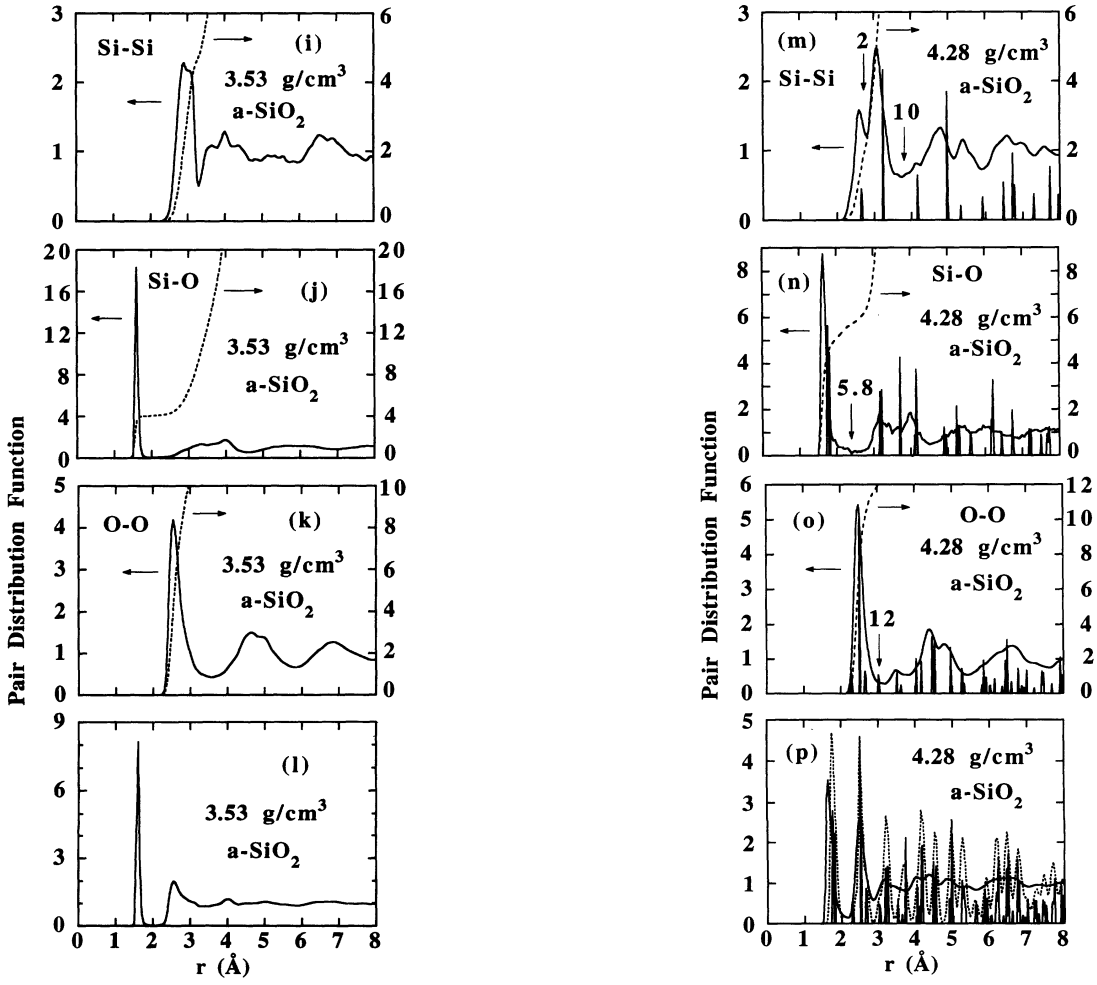

FIG. 1. (*Continued*).

Å which is the next-nearest-neighbor (NNN) Si-O separation. There is a broad peak at 4.16 Å due to third O neighbors. The gap in $g_{Si\text{-}O}(r)$ decreases as density increases and the broad peak shifts to 4.12 and 3.98 Å at 2.94 and 3.53 g/cm^3, respectively. In the glass at 4.28 g/cm^3, the second peak in $g_{Si\text{-}O}(r)$ is at 3.15 Å, close to the NNN Si-O distance (3.20 Å) in stishovite.

Figure 1 also shows how the Si-Si pair distribution function changes upon densification. In the normal and densified glasses at 2.20, 2.94, and 3.53 g/cm^3, the average nearest-neighbor Si-Si distances are 3.09, 3.00, and 2.89 Å, respectively, the average NNN Si-Si distances are 5.00, 4.25, and 4.00 Å, respectively. In the normal-density glass, the nearest-neighbor Si-Si coordination is 4 and it remains 4 even when the density increases to 2.94 g/cm^3. However, at 3.53 g/cm^3, the NN Si-Si coordination changes to 4.8. At the highest density, 4.28 g/cm^3, the first peak in $g_{Si\text{-}Si}(r)$ splits into two peaks located at 2.59 and 3.07 Å. These peaks are close to the NN (2.67 Å) and NNN (3.24 Å) Si-Si separations in stishovite. In the highest-density glass, the area under the first peak gives a coordination of 2 while the area under the first two peaks gives a coordination of 10. In stishovite, the Si-Si coordination is also 10.

Figure 1 also displays changes in the O-O pair distribution function upon densification. At densities of 2.20, 2.94, and 3.53 g/cm^3, the NN O-O separations are 2.65, 2.60, and 2.55 Å, respectively. The second peaks in $g_{O\text{-}O}(r)$ occur at 5.06, 4.84, and 4.63 Å, respectively. In the normal-density glass, the nearest-neighbor O-O coordination is 6. At higher densities, the O-O coordination increases continuously: at 2.94 g/cm^3, $n_{O\text{-}O}(r)=8$, 10, and 12 at $r=3.02$, 3.35, and 3.70 Å, respectively. With further increase in the density to 3.53 g/cm^3, $n_{O\text{-}O}(r)=11$ and 12 at $r=3.12$ and 3.32 Å, respectively. When the glass density reaches 4.28 g/cm^3, the first peak in $g_{O\text{-}O}(r)$ is at 2.50 Å (with a FWHM of 0.27 Å) and the O-O coordination is 12. Note that, in stishovite, the NN O-O coordination is also 12.

Figure 2 displays the distribution of Si-Si, Si-O, O-Si, and O-O nearest neighbors in the normal-density and the highest-density glasses. At the normal density, almost all of the Si atoms have four O nearest neighbors within a cutoff distance of 2.50 Å, and almost all of the O atoms have two Si nearest neighbors with that distance. At the highest density, 86% of Si atoms have six O neighbors within a cutoff distance of 2.64 Å. The remaining Si atoms have 4, 5, 7, and 8 O neighbors. At normal density, 89.4% of the Si atoms have four NN Si atoms within a cutoff distance of 3.50 Å and 85.3% of the O atoms have six NN O atoms within a cutoff distance of 2.93 Å. At the highest density, the Si-Si and O-O coordination distributions are broad and centered around 10 and 12, respectively.

B. Bond-angle distributions

Bond-angle distributions provide valuable information about the local structural units and their connectivity in the glass. Figure 3 displays the distributions $P(\theta_{ijk})$ for bond angles θ_{ijk} in 300 K SiO_2 glasses at $\rho=2.20$, 2.64, 2.94, and 3.53 g/cm^3. Each distribution is an average over 100 configurations at intervals of $100\Delta t$. The bond angles are determined with Si-Si, Si-O, and O-O cutoff distances at the end of the first minima in the corresponding pair distribution functions.

At normal density, the O-Si-O bond-angle distribution has only one well-defined peak, at 109° with a FWHM of 10°. The distributions in $P(\angle\text{O-O-Si})$ and $P(\angle\text{O-O-O})$ have sharp peaks at 35° and 60°, respectively. For an ideal $Si(O_{1/2})_4$ tetrahedron, the O-O-O bond angle is 60°, the O-Si-O bond angle is $\cos^{-1}(-\frac{1}{3})=109.47°$, and the O-O-Si bond angle is 35.26°. The deviations from these ideal bond angles indicate the presence of slightly distorted $Si(O_{1/2})_4$ tetrahedra in the normal-density glass.

As the density increases, the peak in the O-Si-O bond-angle distribution broadens and shifts to a lower angle because of increased distortions of $Si(O_{1/2})_4$ tetrahedra. With a 20% increase in the density, the peak in $P(\angle\text{O-Si-O})$ moves from 109° to 107° and the FWHM increases from 10° to 12° With further increase of the density to 3.53 g/cm^3, the peak shifts to 104° and its FWHM increases to 17°.

In the normal-density glass, the Si-O-Si bond-angle distribution has a single peak at 144° and the FWHM of this peak is 26°. Both of the width and the peak positions are in excellent agreement with magic-angle-spinning nuclear magnetic resonance (MAS-NMR) measurements.[37] The peak position in Si-O-Si bond-angle distribution is a manifestation of a corner-sharing tetrahedral network. With an increase in the density, the peak in Si-O-Si bond-angle distribution broadens and shifts continuously to lower angles: at 2.64 and 2.94 g/cm^3, this peak shifts to 139° and 137°, respectively. With 60% densification (3.53 g/cm^3), the peak occurs at 127° and in addition a broad shoulder appears around 146°. There are no edge-sharing tetrahedra in the glass. The reduction of the Si-O-Si bond angle width an increase in the density is consistent with the decrease in the NN Si-Si distance.

In the normal-density glass, the Si-Si-Si bond angle has a broad distribution centered around 105°. There is a small peak at 60° due to threefold rings. As the density increases, the broad band moves to lower angles and the peak at 60° grows. In the normal-density system, the Si-Si-O bond-angle distribution has a narrow peak at 19°, a broad peak at 100°, and a shoulder around 120°. The O-O-Si bond-angle distribution has a sharp peak at 35° and a broad band between 85° and 180°. The O-O-O bond-angle distribution has a sharp peak at 60° followed by a broad band between 70° and 180°. As the density increases from 2.20 to 3.53 g/cm^3, the peak at 19° in Si-Si-O bond-angle distribution shifts to larger angles, its width increases, and its height decreases. The sharp peak in O-O-Si bond-angle distributions manifests similar changes. In the O-O-O bond-angle distribution, the first peak remains at 60° when the density is increased from 2.20 to 3.53 g/cm^3. In the Si-Si-O bond-angle distribution, the width of the broad peak around 100° increases and its height decreases. In addition, upon densification to 3.53 g/cm^3, the Si-Si-O bond-angle distribution has a shoulder at 18°, the O-O-Si bond-angle distribution has a broad

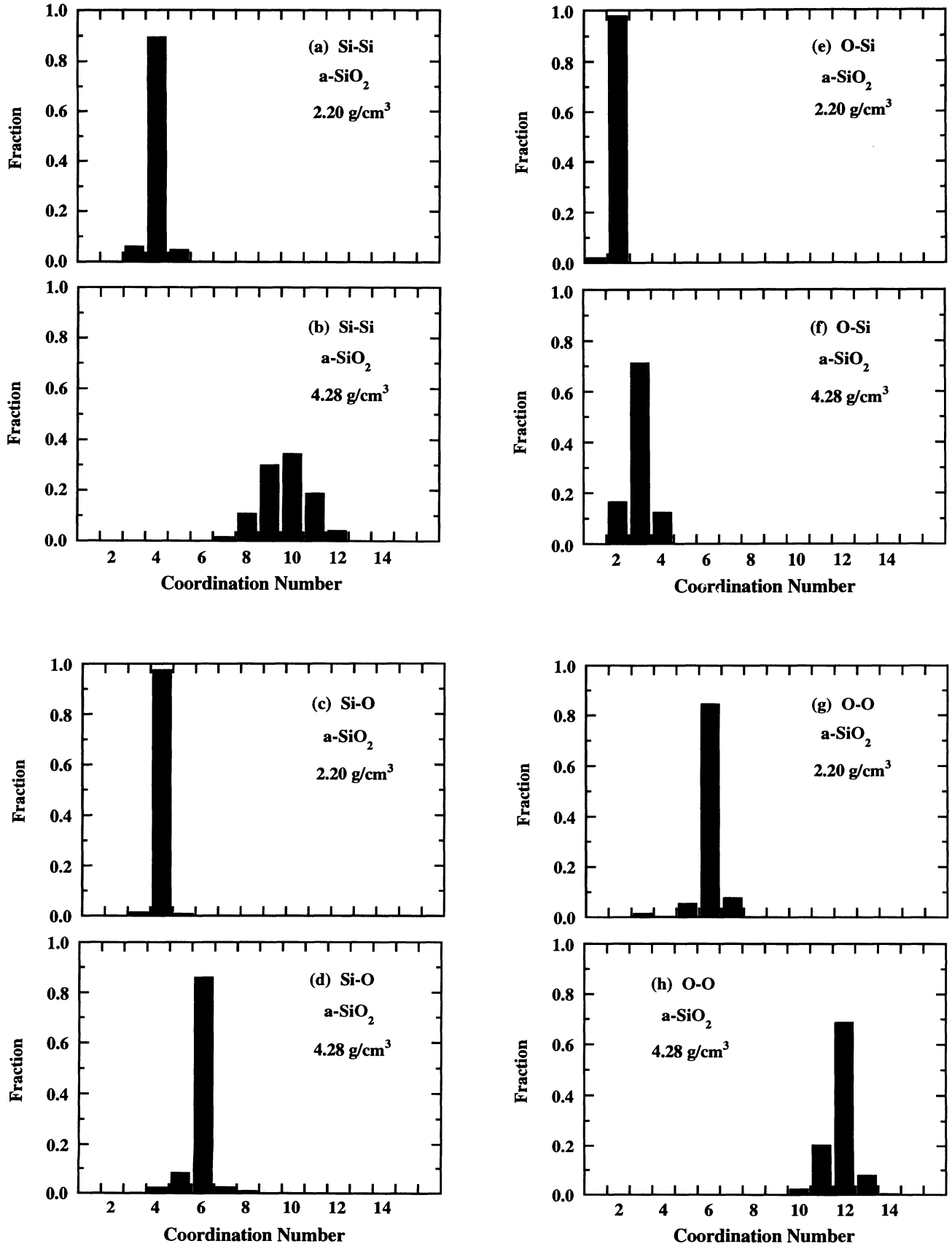

FIG. 2. Distributions of Si and O nearest-neighbor coordinations in SiO_2 glass at 2.20 and 4.28 g/cm^3. In the horizontal axis, each cell represents a coordination category. Vertical bars in each cell represent percentages of a particular coordination.

peak around 90°, and the O-O-O bond-angle distribution has a broad peak around 110°.

Bond-angle distributions undergo dramatic changes when the glass density is increased to 4.28 g/cm^3. Figure 4 compares the bond-angle distributions in the highest-density glass and in stishovite. The Si-O-Si bond-angle distribution in the highest-density glass has broad peaks at 95° and 128°. Note that these values are close to the Si-O-Si angles, 98.65° and 130.67°, in stishovite. The O-Si-O bond-angle distribution in the highest-density glass has broad peaks at 90° and 180°. In stishovite, the O-Si-O angles are 81.35°, 90°, 98.65°, and 180°. The Si-Si-Si bond-angle distribution in the highest-density glass displays a broad band between 35° and 180°, with several superimposed features which are close to the peak positions in the stishovite. Figures 4(b), 4(e), and 4(f) also show that peaks in $P(\angle$Si-Si-O), $P(\angle$O-O-Si), and $P(\angle$O-O-O) for the highest-density glass are close to the peak positions for stishovite. The peaks at 46°, 90°, and 134° in $P(\angle$Si-Si-O) for both the highest-density glass and stishovite involve the two NN Si-Si atoms while all other peaks in $P(\angle$Si-Si-O) involve the eight NNN Si-Si atoms.

Figure 5 shows a snapshot of typical structural units and their connectivity in the network glass at 4.28 g/cm^3. Clearly, the system has $Si(O_{1/3})_6$ octahedral structural units which share corners as well as edges. The 18 atomic positions in the octahedra are given in Table I. Most of the features in bond-angle distributions at 4.28 g/cm^3 can be understood by examining angles of the octahedra in Fig. 5. The Si-Si-Si bond angles in Fig. 5 are calculated

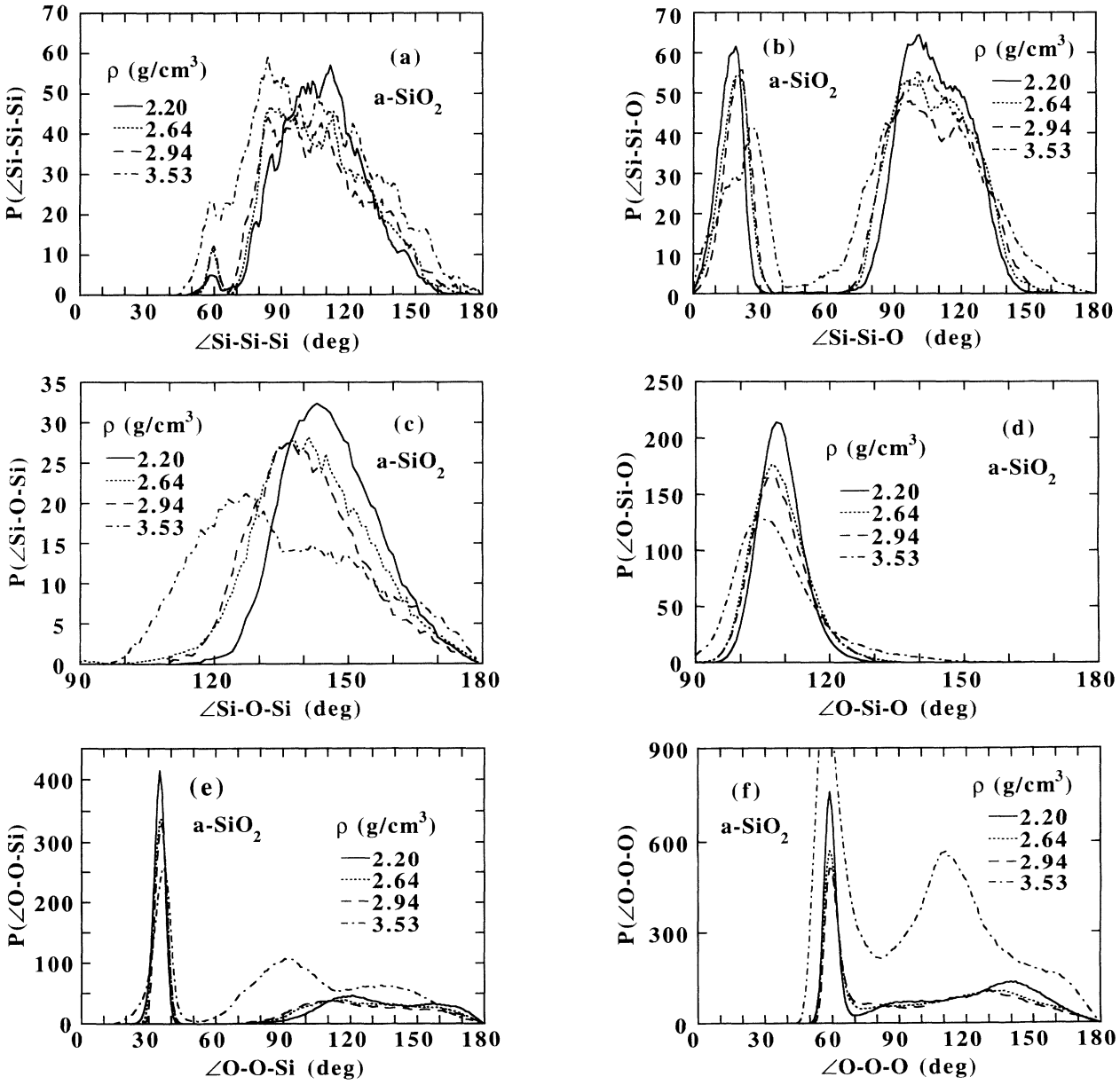

FIG. 3. (a) Si-Si-Si, (b) Si-Si-O, (c) Si-O-Si, (d) O-Si-O, (e) O-O-Si, and (f) O-O-O bond-angle distributions for SiO_2 glasses at densities of 2.20 g/cm^3 (solid lines), 2.64 g/cm^3 (short-dashed lines), 2.94 g/cm^3 (long-dashed lines), and 3.53 g/cm^3 (dot-dashed lines).

to be 53.5°, 59.2°, and 67.4°, which are in agreement with the position at 65° in $P(\angle\text{Si-Si-Si})$ [Fig. 4(a)]. The Si-Si distance between the two Si atoms of the two edge-sharing octahedra in Fig. 5 is 2.74 Å, falls within the first peak of $g_{\text{Si-Si}}(r)$ [Fig. 1(m)]. The distances of these two Si atoms to the third Si atom are 2.93 and 3.15 Å, close to the second peak in $g_{\text{Si-Si}}(r)$. The Si-O-Si bond angles in Fig. 5 are 97.1°, 124.4°, and 132.4°, in agreement with the peaks in Fig. 4(c). In Fig. 5, there are 36 Si-Si-O bond angles. For example, some of these bond angles are calculated to be 23.1°, 35.6°, 44.8°, 73.1°, 81.7°, 103.1°, 121.0°, and 158.0°, etc. Indeed, there are peaks around 22°, 40°, 80°, 110°, 135°, and 155° in Fig. 4(b). Similarly, calculations for the O-Si-O, O-O-Si, and O-O-O bond angles in the three octahedra are consistent with the MD results.

C. Static structure factors and comparison between simulation and experimental results

To compare with available diffraction experiments, we have calculated the total static structure factors from partial static structure factors. The latter are calculated through Fourier transforms of partial pair distribution functions,

$$S_{\alpha\beta}(q)=\delta_{\alpha\beta}+4\pi n(c_\alpha c_\beta)^{1/2} \times\int_0^\infty [g_{\alpha\beta}(r)-1]\frac{\sin(qr)}{qr}r^2dr\ . \tag{7}$$

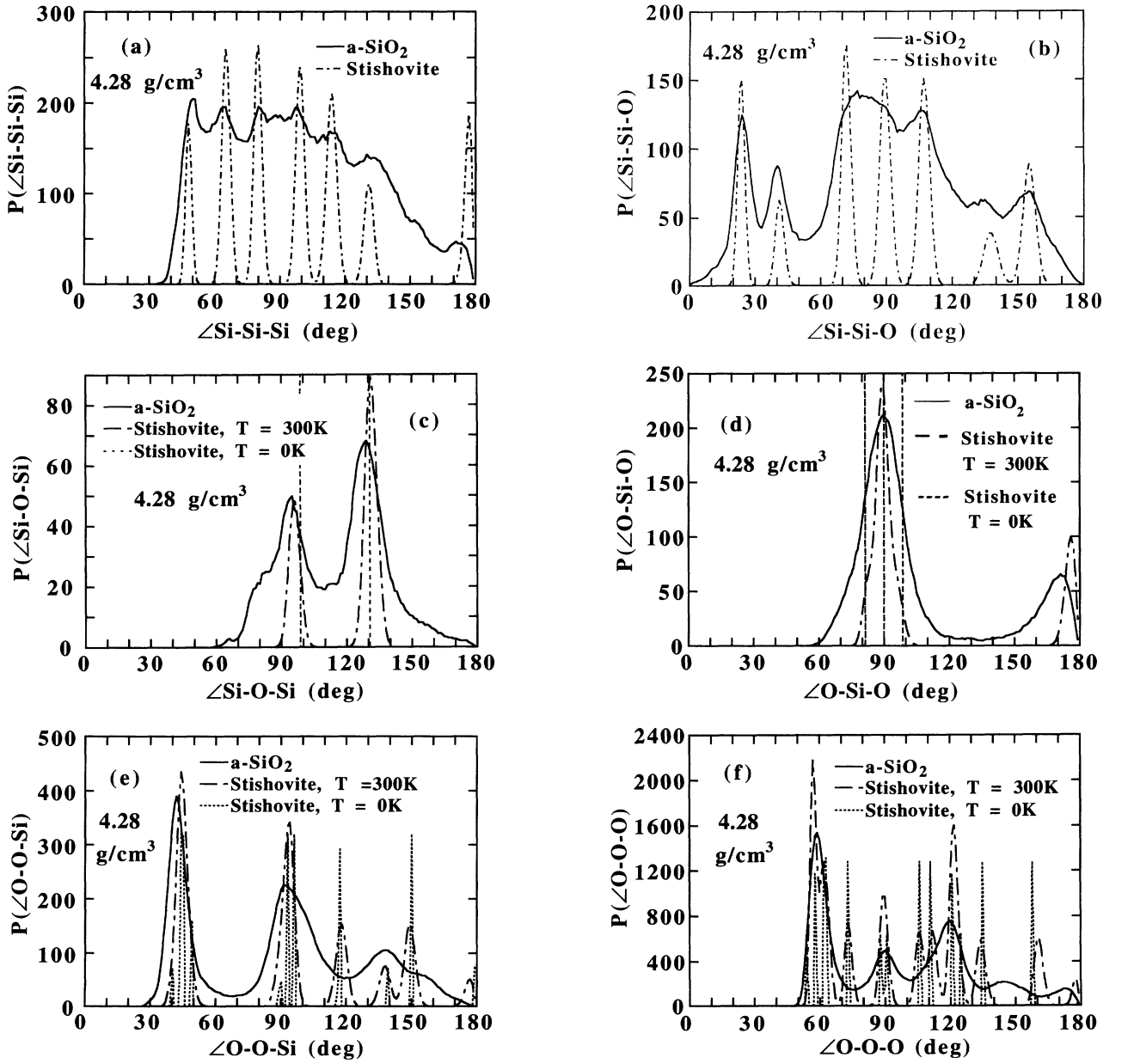

FIG. 4. (a) Si-Si-Si, (b) Si-Si-O, (c) Si-O-Si, (d) O-Si-O, (e) O-O-Si, and (f) O-O-O bond-angle distributions for the highest-density (4.28 g/cm³) SiO_2 glass at 300 K (solid lines) and for stishovite. The dot-dashed lines in (a)–(f) are the bond-angle distributions for stishovite at 300 K, and the vertical short-dashed lines in (c) and (d) are the bond-angle distributions for stishovite at zero temperature.

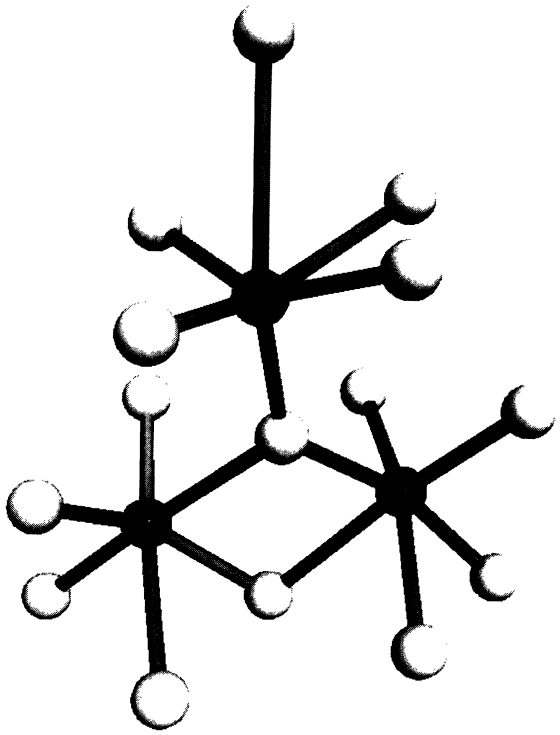

FIG. 5. Arrangement of Si (light spheres) and O (dark spheres) atoms in three Si $(O_{1/3})_6$ octahedra taken from an instantaneous configuration of the highest-density (4.28 g/cm^3) SiO_2 glass obtained in our MD simulation. The bonds connect nearest-neighbor Si-O atoms. The lower two $Si(O_{1/3})_6$ octahedra share one common O-O edge. The upper octahedron shares one common vortex O atom with the lower two octahedra.

TABLE I. Atomic positions and Si-O nearest-neighbor connectivity in three octahedra (shown in Fig. 5), taken from an instantaneous MD configuration of the highest-density (4.28 g/cm^3) glass. The first three atoms are Si, each belonging to one octahedron. The remaining fifteen atoms are O. Atom no. 6 is the common-vertex O atom shared by the three octahedra. Atom no. 12 is shared by the lower two octahedra.

Atomic index	Positions (Å)			Connectivity
	x	y	z	
1	9.844	10.22	14.53	4 6 9 10 12 14
2	7.743	8.474	14.75	5 6 11 12 15 17
3	72.94	11.58	15.00	6 7 8 13 16 18
4	10.25	9.886	16.51	1
5	7.221	9.002	13.33	2
6	8.280	10.38	15.02	1 2 3
7	6.224	11.15	13.82	3
8	8.365	12.56	13.13	3
9	10.22	11.90	14.81	1
10	11.39	9.814	14.49	1
11	7.339	6.820	14.60	2
12	9.356	8.333	14.72	1 2
13	6.092	13.50	14.21	3
14	9.355	10.21	12.88	1
15	6.516	8.776	15.74	2
16	6.410	11.40	16.35	3
17	8.286	8.456	17.11	2
18	8.126	12.84	15.62	3

The total static structure factor is given by

$$S(q)=\sum_{\alpha}\sum_{\beta}(c_\alpha c_\beta)^{1/2}S_{\alpha\beta}(q)\ . \tag{8}$$

Figure 6 displays the computed partial static structure factors for the normal and densified glasses at 300 K. For comparison, the computed partial static structure factors for stishovite are also shown in Figs. 6(d)–6(f). At normal density, the first peaks in $S_{\text{Si-Si}}(q)$ and $S_{\text{O-O}}(q)$ occur at 1.67 and 1.61 Å^{-1}, respectively, while the largest (second) peaks are at 2.67 and 2.78 Å^{-1}, respectively. In $S_{\text{Si-O}}(q)$, there is a small peak at 1.61 Å^{-1}, followed by a deep minimum at 2.72 Å^{-1}. As the density increases from 2.20 to 3.53 g/cm^3, the first two peaks in $S_{\text{Si-Si}}(q)$ and $S_{\text{O-O}}(q)$ and the drop in $S_{\text{Si-O}}(q)$ shift slightly to higher values of q [Figs. 6(a)–6(c)]. At each density, the largest peaks in $S_{\text{Si-Si}}(q)$ and $S_{\text{O-O}}(q)$ and the deep minimum in $S_{\text{Si-O}}(q)$ occur almost at the same values of q. At the highest density (Fig. 6), the first peaks in $S_{\text{Si-Si}}(q)$ and $S_{\text{O-O}}(q)$ have almost disappeared.

Figure 7 presents the MD results for the total static structure factors at different densities. Clearly, the densification has a profound effect on the FSDP but not much on peaks at higher values of q. Figure 8 displays the density dependence of the position and height of the first two peaks in $S(q)$. In the normal-density glass, the FSDP is located at 1.60 Å^{-1}. With an increase in the density, the height of the FSDP decreases, its width increases, and its position shifts to higher values of q. Note that simple elastic compression [i.e., $(\rho/\rho_0)^{1/3}=L_0/L$] cannot account for the observed shift in the position of the FSDP. Elastic compression corresponding to density increases of 20%, 33%, 60%, and 95% would shift the FSDP to 1.71, 1.77, 1.88, and 2.01 Å^{-1}, whereas the simulation results reveal higher values for the position of the FSDP: 1.85, 1.94, 2.15, and 2.19 Å^{-1}. The MD simulation results for the shift and loss of the FSDP are in agreement with the recent high-pressure x-ray measurements of Meade, Hemley, and Mao.[9]

Figure 7 also shows a "new" peak in the static structure factor. It appears when the density of the normal system is increased by 20%. Located at 2.85 Å^{-1}, the peak grows with increase in the density. However, its position shifts only slightly at higher pressures [Fig. 8(a)]. These results are again in agreement with the recent x-ray measurements at high pressures.[9]

The major structural probes of amorphous materials are neutron and x-ray diffraction.[36] High-quality neutron diffraction data are available for SiO_2 glass under ambient conditions.[34] However, high-pressure neutron measurements have not yet been carried out. Only Susman *et al.*[11] have reported diffraction measurements on 20% densified SiO_2 glass samples recovered from a 16-GPa compression at room temperature.

Neutron diffraction experiments provide a neutron static structure factor $S_n(q)$ [or neutron interference function $qI_n(q)$], and real-space correlations such as the

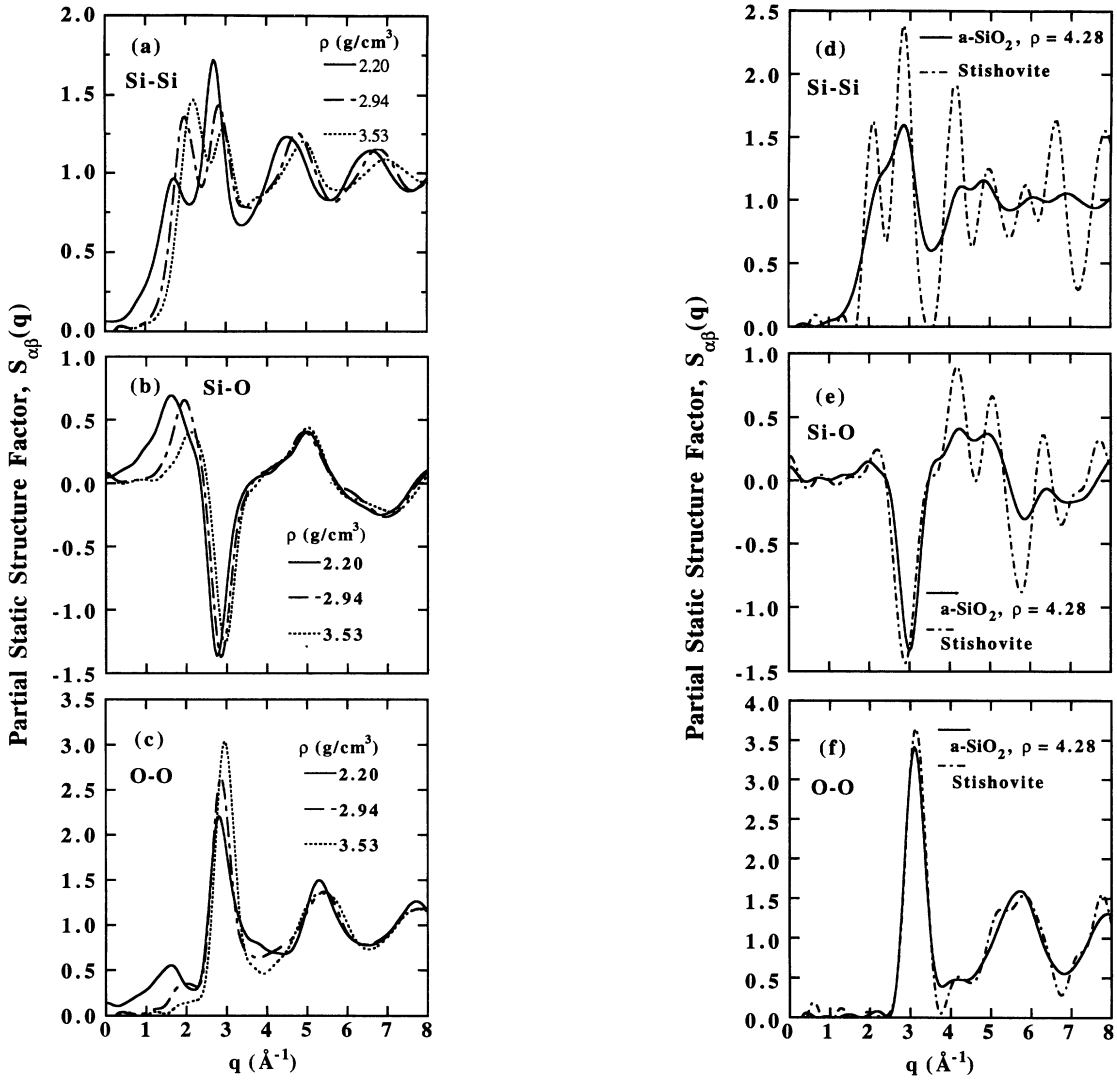

FIG. 6. Si-Si (a), (d), Si-O (b), (e), and O-O (c), (f) partial static structure factors for normal- and high-density SiO_2 glasses and for stishovite at 300 K.

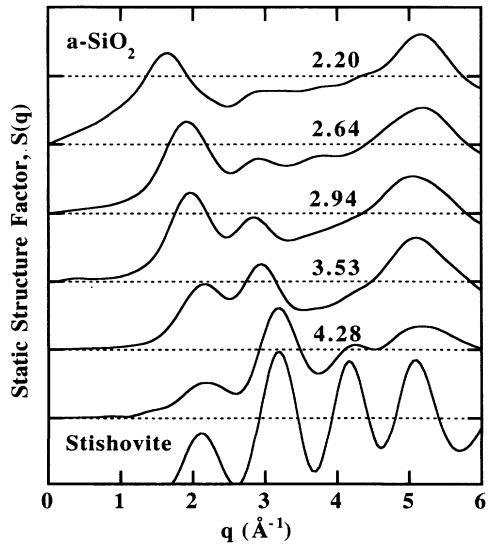

FIG. 7. Total static structure factors for normal- and high-density SiO_2 glasses and for stishovite at 300 K. The first sharp diffraction peak in the normal density glass is at 1.60 $Å^{-1}$.

effective neutron-weighted pair distribution function,

$$g_n(r)=\frac{\sum_\alpha\sum_\beta c_\alpha c_\beta b_\alpha b_\beta g_{\alpha\beta}(r)}{\left[\sum_\alpha c_\alpha b_\alpha\right]^2}\ , \tag{9}$$

the total neutron correlation function $t(r)$, and diffraction function $d(r)$,

$$t(r)=4\pi n r g_n(r)\ , \tag{10}$$

$$d(r)=t(r)-4\pi n r\ . \tag{11}$$

Here b_α is the coherent neutron scattering length of atoms of type α. In molecular-dynamics simulation, the neutron interference function can be calculated from

$$qI_n(q)=\int_0^\infty d(r)\sin(qr)dr\ , \tag{12}$$

and the neutron static structure factor from[44]

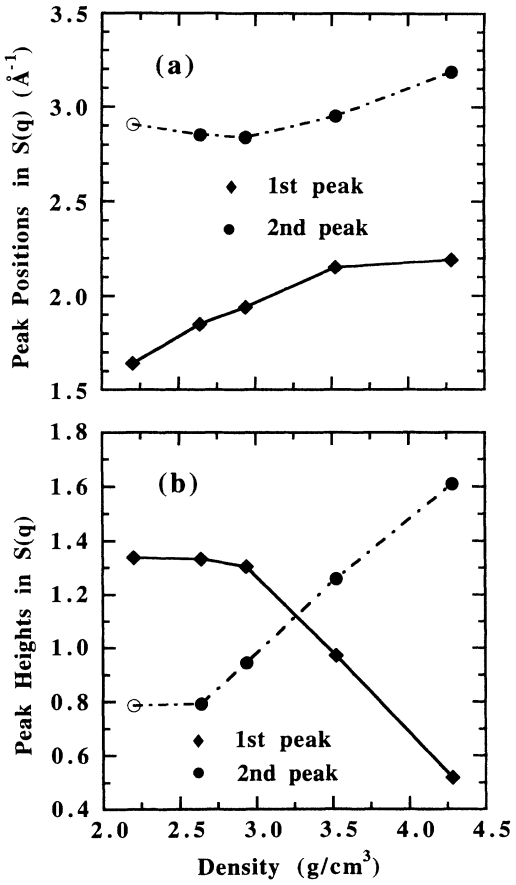

FIG. 8. Density dependencies of (a) positions and (b) heights of the first (♦) and second (●) peaks in the total static structure factor of SiO_2 glass. Open circles (○) at normal density are meant to indicate that the second peak is broad and has a small amplitude.

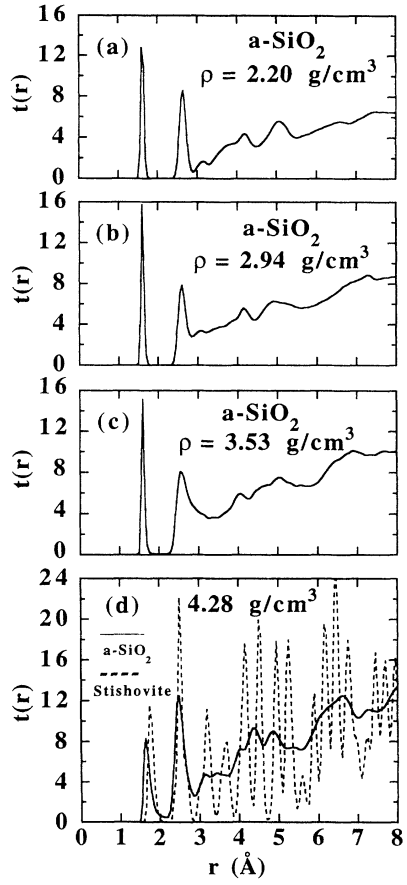

FIG. 9. Total neutron correlation function $t(r)$ for SiO_2 glasses at (a) 2.20, (b) 2.94, (c) 3.53, and (d) 4.28 g/cm^3 at 300 K. The dashed line in (d) is the neutron correlation function for stishovite at 300 K.

$$S_n(q)=\sum_\alpha\sum_\beta b_\alpha b_\beta (c_\alpha c_\beta)^{1/2}[S_{\alpha\beta}(q)-\delta_{\alpha\beta}+(c_\alpha c_\beta)^{1/2}]\Big/\left[\sum_\alpha b_\alpha c_\alpha\right]^2 . \tag{13}$$

$S_n(q)$ and $qI_n(q)$ are related by

$$qI_n(q)=q[S_n(q)-1] . \tag{14}$$

Figure 9 displays the calculated $t(r)$ at various densities. For comparison, the corresponding results for stishovite at 300 K are also shown. For the normal-density system [Fig. 9(a)], the peaks at 1.61 and 2.65 Å reflect the NN Si-O and NN O-O separations, respectively. The small peaks at 3.09 and 4.27 Å arise from the NN Si-Si and NNN Si-O correlations, respectively. The peak at 5.05 Å is due to the NNN Si-Si and NNN O-O separations. In the glass at 4.28 g/cm^3, the first peak in $t(r)$ at 1.67 Å is due to the NN Si-O separation. The second peak in $t(r)$ at 2.50 Å is due to the NN Si-Si and NN O-O separations. Note that, in stishovite, the first peak is at 1.80 Å and the second peak is at 2.50 Å.

Figure 10 displays the neutron static structure factors at various densities. The experimental results for a-SiO_2 at 2.20 g/cm^3 (normal system) and 2.64 g/cm^3 (20% densified system) are also shown in figure. The latter are the only available neutron diffraction data on densified a-SiO_2. The calculated $S_n(q)$ are in good agreement with neutron measurements. In the normal-density system, the prominent features in the calculated $S_n(q)$ are peaks at 1.60, 2.85, 5.20, 7.72, and 12.33 Å^{-1} and shoulders around 9.75 and 15.05 Å^{-1}. From the partial static structure factor [Figs. 6(a), 6(b), and 6(c)], it is evident that the second peak at 2.85 Å^{-1} is due to the Si-Si and O-O structure factors with partial cancellation arising from the Si-O structure factor. The largest peak at 5.11 Å^{-1} is due to all three partial structure factors. As the density increases, the height of the first peak in $S_n(q)$ de-

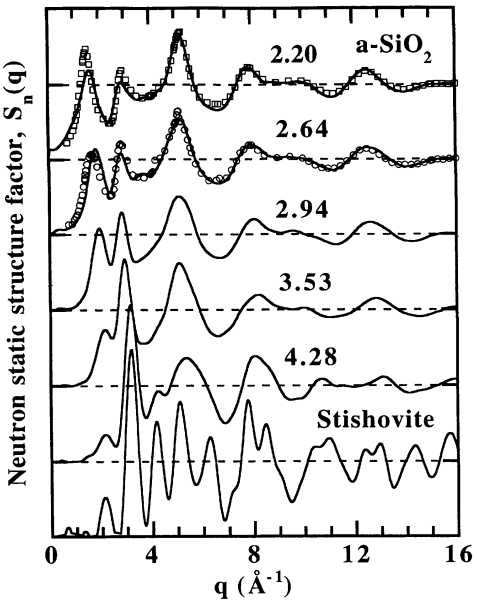

FIG. 10. Neutron-weighted static factors for normal- and high-density SiO_2 glasses and for stishovite. The first sharp diffraction peak in the normal-density glass is at 1.60 Å^{-1}. Solid lines are MD results at 300 K; open squares (□) and open circles (○) are the neutron diffraction experimental results. The lower height of the FSDP from MD simulations is entirely due to the size effect of the system (Ref. 40).

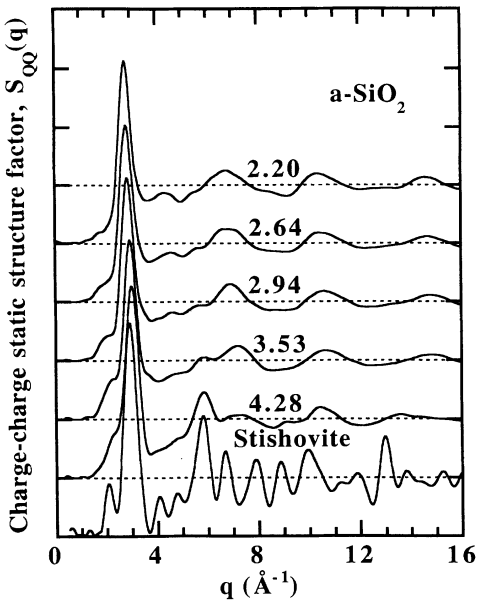

FIG. 11. Total charge-charge static structure factors for normal- and high-density SiO_2 glasses and for stishovite at 300 K.

creases and the height of the second peak increases. The FSDP shifts from 1.60 Å^{-1} to 1.85, 1.94, 2.15, and 2.19 Å^{-1} with 20%, 33%, 60%, and 95% densification, respectively. The second peak shifts to 2.83, 2.84, 2.94, and 3.16 Å^{-1}, respectively.

We have also investigated the behavior of the total charge-charge static structure factor $S_{QQ}(q)$,[40]

$$S_{QQ}(q)=\sum_{\alpha}\sum_{\beta}\frac{Q_\alpha Q_\beta}{\langle Q^2\rangle}(c_\alpha c_\beta)^{1/2}S_{\alpha\beta}(q)\ , \tag{15}$$

and the corresponding real-space total charge-charge correlation function

$$g_{QQ}(r)=\sum_{\alpha}\sum_{\beta}\frac{Q_\alpha Q_\beta}{\langle Q^2\rangle}c_\alpha c_\beta g_{\alpha\beta}(r)\ , \tag{16}$$

where $\langle Q^2\rangle=\sum_\alpha c_\alpha Q_\alpha^2$.

Figure 11 displays the computed total charge-charge static structure factors for SiO_2 glasses and stishovite at 300 K. The peaks in $S_{QQ}(q)$ are roughly out of phase with the peaks in $S_n(q)$. Unlike $S(q)$ or $S_n(q)$, $S_{QQ}(q)$ does not have a FSDP. In the normal-density glass, the first peak in $S_{QQ}(q)$ occurs at 2.72 Å^{-1} and there are weaker peaks at 4.35, 6.74, 10.38, and 14.56 Å^{-1}. As the density increases, these peaks shift to larger values of q: in the glasses at 2.24, 2.94, 3.53, and 4.28 g/cm^3, the first peak occurs at 2.79, 2.82, 2.93, and 2.98 Å^{-1}. In addition, a peak appears at 5.84 Å^{-1} in the glass at 4.28 g/cm^3.

D. Ring statistic and oxygen packing fraction

Often, the network topology of a covalent glass is analyzed in terms of ring statistics.[45–47] A ring is defined by the *shortest closed path* made of Si-O bonds for a give Si atom. With this definition, α- and β-cristobalites are composed of only sixfold rings, whereas α- and β-quartz have four sixfold and two eightfold rings per Si atom. In coesite, there are four-, six-, and eightfold rings. For glasses below 3.53 g/cm^3, each Si is fourfold coordinated and so the maximum possible number of rings per Si atom is $4\times\frac{3}{2}=6$. For glass at 4.28 g/cm^3, the majority of the Si atoms are sixfold coordinated so that the maximum possible number of rings per Si atom is $6\times\frac{5}{2}=15$.

We have calculated the population of rings of size 2–11 using 100 MD configurations at intervals of 100 time steps. Distributions of interatomic distances and bond angles in these rings have also been calculated. In the normal-density system, the population of twofold to elevenfold rings per Si atom is 0.0, 0.0556, 0.5278, 1.4150, 2.1363, 1.1804, 0.3763, 0.0564, 0.0046, and 0.0, respectively. The distribution is peaked at sixfold rings and is nearly symmetric. At 3.53 g/cm^3, the population of twofold to elevenfold rings per Si atom is 0.0, 0.0919, 0.7600, 1.5735, 1.5637, 1.3594, 0.3911, 0.0526, 0.0001, and 0.0, respectively. The distribution is still dominated by five-, six-, and sevenfold rings. There are no twofold rings and a very small number (1%) of threefold rings. However, at 4.28 g/cm^3, a large number of two-, three-, four-, five-, and sixfold rings (3.2313, 6.3098, 4.4209, 0.6730, and 0.0196 per Si atom, respectively) are found. This is similar to the ring distribution in stishovite, which has two twofold, ten threefold, and three fourfold rings per Si atom.

The network structure can also be analyzed in terms of

the *effective* volume occupied by O atoms. Since O atoms occupy most of the volume, we calculate their volume fraction p, assuming that an O atom is a sphere of diameter d,

$$p=\frac{N_O}{L^3}\left[\frac{4\pi}{3}\right]\left[\frac{d}{2}\right]^3,$$

where $N_O=432$ is the total number of O atoms in the MD system. Taking d to be the average NN O-O distance calculated from the position of the first peak in $g_{O\text{-}O}(r)$, we obtain $p=0.431$ in the normal-density glass. The value of p increases to 0.482, 0.543, 0.613, and 0.699 at densities of 2.64, 2.94, 3.53, and 4.28 g/cm^3, respectively. Note that for *random close packing* (RCP) of hard spheres, the volume packing fraction is 0.637, while for *regular dense packing*, the packing fraction is $\sqrt{2}\pi/6=0.740$. Thus, glasses up to 33% densification are open networks and the glass with 60% densification has nearly the same packing fraction as the RCP of oxygen atoms. This is also consistent with the increase in the O-O-O bond-angle distributions near 60° and 120° [Fig. 3(f)]. The increase in oxygen packing and the concomitant decrease in the Si-O-Si bond angle upon densification increase the frustration associated with the packing of $Si(O_{1/2})_4$ tetrahedra.[48] This increasing frustration causes the reduction of the intermediate-range order in the high-density glasses.

IV. SUMMARY

We have investigated via molecular-dynamics simulations the microscopic structures in densified SiO_2 glasses. The results of pair distribution functions, coordination numbers, bond-angle distributions, and ring statistics show that up to 60% densification the $Si(O_{1/2})_4$ tetrahedra structural unit remains intact and structural change is associated with bending and distortion of the tetrahedra. Further compression increases the Si-O coordination from tetrahedral to nearly octahedral (Si-O NN coordination 5.8) and the glass undergoes a transformation from a corner-sharing $Si(O_{1/2})_4$ tetrahedral network to a network of predominantly $Si(O_{1/3})_6$ octahedra joined at corners and edges. The MD simulations also show that, as the density increases, the FSDP decreases in height, shifts to larger values of q, and a new peak appears. This peak grows as the density increases. The shift in the FSDP is larger than the one produced by simple elastic compression. These results are in good agreement with the recent high-pressure x-ray diffraction measurements on SiO_2 glass.

ACKNOWLEDGMENTS

We thank Dr. S. W. de Leeuw, Dr. A. Nakano, and Dr. J. Yu for helpful discussions. This work was supported by the U.S. Department of Energy, Office of Energy Research, Basic Energy Sciences, Materials Sciences Division, Grant No. DE-FG05-92ER45477. The computations were performed using the computing facilities in the Concurrent Computing Laboratory for Materials Simulations (CCLMS) at Louisiana State University. The facilities in the CCLMS were acquired with Equipment Enhancement Grants awarded by the Louisiana Board of Regents through Louisiana Education Quality Support Fund (LEQSF).

[1] K. Tanaka, J. Non-Cryst. Solids **90**, 363 (1987).
[2] L. Liu and W. A. Basset, *Elements, Oxides, Silicates: High-Pressure Phases with Implications for the Earth's Interior* (Oxford University, New York, 1986).
[3] M. Grimsditch, R. Bhadra, and Y. Meng, Phys. Rev. B **38**, 7836 (1988); J. P. Itie *et al.*, Phys. Rev. Lett. **63**, 398 (1989); D. J. Durben and G. H. Wolf, Phys. Rev. B **43**, 2355 (1991).
[4] M. Grimsditch, Phys. Rev. Lett. **52**, 2379 (1984); Phys. Rev. B **34**, 4372 (1986); A. Polian and M. Grimsditch, *ibid.* **41**, 6086 (1990).
[5] R. J. Hemley, H. K. Mao, P. M. Bell, and B. O. Mysen, Phys. Rev. Lett. **57**, 747 (1986).
[6] P. McMillian, B. Piriou, and R. Couty, J. Chem. Phys. **81**, 4234 (1984); B. Velde and R. Couty, J. Non-Cryst. Solids **94**, 238 (1987).
[7] C. Meade and R. Jeanloz, Phys. Rev. B **35**, 236 (1987).
[8] Q. Williams and R. Jeanloz, Science **239**, 902 (1988).
[9] C. Meade, R. J. Hemley, and H. K. Mao, Phys. Rev. Lett. **69**, 1387 (1992).
[10] L. E. McNeil and M. Grimsditch, Phys. Rev. Lett. **68**, 83 (1992).
[11] S. Susman *et al.*, Phys. Rev. B **43**, 1194 (1991).
[12] R. J. Hemley *et al.*, Nature **334**, 52 (1988).
[13] A. J. Gratz, L. D. DeLoach, T. M. Clough, and W. J. Nellis, Science **259**, 663 (1993).
[14] K. J. Kingma, C. Meade, R. J. Hemley, H. K. Mao, and D. R. Veblen, Science **259**, 666 (1993).
[15] L. V. Woodcock, C. A. Angell, and P. Cheeseman, J. Chem. Phys. **65**, 1565 (1976).
[16] R. A. Murray and W. Y. Ching, Phys. Rev. B **39**, 1320 (1989).
[17] J. S. Tse and D. D. Klug, J. Chem. Phys. **95**, 9176 (1991); Phys. Rev. Lett. **67**, 3559 (1991); **70**, 174 (1993); J. S. Tse, D. D. Klug, and Y. Le Page, Phys. Rev. B **46**, 5933 (1992).
[18] J. R. Rustad, D. A. Yuen, and F. J. Spera, Phys. Rev. B **44**, 2108 (1991).
[19] S. Tsuneyuki, M. Tsukada, H. Aoki, and Y. Matsui, Phys. Rev. Lett. **61**, 869 (1988); S. Tsuneyuki, Y. Matsui, H. Aoki, and M. Tsukada, Nature **339**, 209 (1989).
[20] Y. Tsuchida and T. Yagi, Nature **340**, 217 (1989).
[21] N. R. Keskar, N. Troullier, J. L. Martins, and J. R. Chelikowsky, Phys. Rev. B **44**, 4081 (1991).
[22] J. R. Chelikowsky, N. Troullier, J. L. Martins, and H. E. Kin, Jr., Phys. Rev. B **44**, 489 (1991); N. Binggeli and J. R. Chelikowsky, Nature **353**, 344 (1991); Phys. Rev. Lett. **69**, 2220 (1992).
[23] S. H. Garofalini, J. Chem. Phys. **76**, 3189 (1982); L. Stixrude and M. S. T. Bukowinski, Phys. Rev. B **44**, 2523 (1991).
[24] J. D. Kubicki, R. J. Hemley, and A. M. Hofmeister, Am.

Mineral. **77**, 258 (1992).

[25]J. Zarzycki, *Glasses and the Vitreous States* (Cambridge University, New York, 1991).

[26]R. W. G. Wyckoff, *Crystal Structures* (Wiley, New York, 1965), Vol. 1, pp. 313–322.

[27]F. Liebau, in *The Physics and Technology of Amorphous SiO_2,* edited by R. A. B. Devine (Plenum, New York, 1968), p. 15.

[28]J. A. E. Desa *et al.*, J. Non-Cryst. Solids **51**, 57 (1982).

[29]J. J. Pluth, J. V. Smith, and J. Faber, Jr., J. Appl. Phys. **57**, 1045 (1985).

[30]L. Levien, C. T. Prewitt, and D. J. Weidner, Am. Mineral. **65**, 920 (1980).

[31]S. C. Moss and D. L. Price, in *Physics of Disordered Materials,* edited by D. Adler, H. Fritzsche, and S. R. Ovshinsky (Plenum, New York, 1985), p. 77; S. R. Elliot, Nature **354**, 445 (1991); S. Susman *et al.*, Phys. Rev. B **43**, 11 076 (1991).

[32]L. Levien and C. T. Prewitt, Am. Mineral. **66**, 324 (1981).

[33]Stishovite possesses a tetragonal structure which belongs to the D_{14}^{4h} space group. The lattice constants are $a=b=4.180$ Å and $c=2.666$ Å. Each unit cell contains two formula units. [L. Liu, W. A. Bassett, and T. Takahashi, J. Geophys. Res. **79**, 1160 (1974).]

[34]R. N. Sinclair and A. C. Wright, J. Non-Cryst. Solids **57**, 447 (1983); P. A. V. Johnson, A. C. Wright, and R. N. Sinclair, *ibid.* **58**, 109 (1983); D. I. Grimley, A. C. Wright, and R. N. Sinclair, *ibid.* **119**, 49 (1990).

[35]R. L. Mozzi and B. E. Warren, J. Appl. Crystallogr. **2**, 164 (1969).

[36]A. C. Wright, J. Non-Cryst. Solids **106**, 1 (1988).

[37]R. Dupree and R. F. Pettifer, Nature **308**, 523 (1984); R. F. Pettifer, R. Dupree, I. Farnan, and U. Steinberg, J. Non-Cryst. **106**, 408 (1988).

[38]E. B. Christiansen *et al.*, J. Am. Ceram. Soc. **45**, 172 (1962); J. D. Mackenzie, *ibid.* **46**, 461 (1963); S. Sakka and J. D. Mackenzie, J. Non-Cryst. Solids **1**, 107 (1969); J. Arndt, J. Am. Ceram. Soc. **52**, 285 (1969); Phys. Chem. Glasses **24**, 104 (1983); R. Bruckner, J. Non-Cryst. Solids **5**, 123 (1970); A. G. Revesz *ibid.* **7**, 77 (1972); A. J. Leadbetter and A. C. Wright, Phys. Chem. Glasses **18**, 79 (1977).

[39]W. Jin, J. P. Rino, P. Vashishta, R. K. Kalia, and A. Nakano, in *Strongly Coupled Plasma Physics,* edited by H. M. Van Horn and S. Ichirmaru (University of Rochester, Rochester, 1993), p. 35; W. Jin, R. K. Kalia, and P. Vashishta, Bull. Am. Phys. Soc. **38**, 675 (1993); W. Jin, R. K. Kalia, P. Vashishta, and J. P. Rino, Phys. Rev. Lett. **71**, 3146 (1993).

[40]P. Vashishta, R. K. Kalia, J. P. Rino, and I. Ebbsojö, Phys. Rev. B **41**, 12 197 (1990); W. Jin, P. Vashishta, R. K. Kalia, and J. P. Rino, *ibid.* **48**, 9359 (1993); A. Nakano, R. K. Kalia, and P. Vashishta, J. Non-Cryst. Solids (to be published).

[41]A. Rahman and P. Vashishta, in *The Physics of Superionic Conductors and Electrode Materials,* edited by J. W. Perram (Plenum, New York, 1983), p. 93.

[42]For glasses at 3.53 and 4.28 g/cm^3 and for stishovite, the three-body force is set to zero.

[43]R. Fletcher, *Practical Methods of Optimiztion* (Wiley, New York, 1980).

[44]S. Susman *et al.*, J. Non-Cryst. Solids **106**, 26 (1988).

[45]A. C. Wright and J. A. E. Desa, Phys. Chem. Glasses **19**, 140 (1978).

[46]B. Feuston and S. H. Garofalini, J. Chem. Phys. **89**, 5818 (1988).

[47]J. P. Rino, I. Ebbsojö, R. K. Kalia, A. Nakano, and P. Vashishta, Phys. Rev. B **47**, 3053 (1993).

[48]S. Susman, K. J. Volin, D. G. Montague, and D. L. Price, J. Non-Cryst. Solids **125**, 168 (1990).

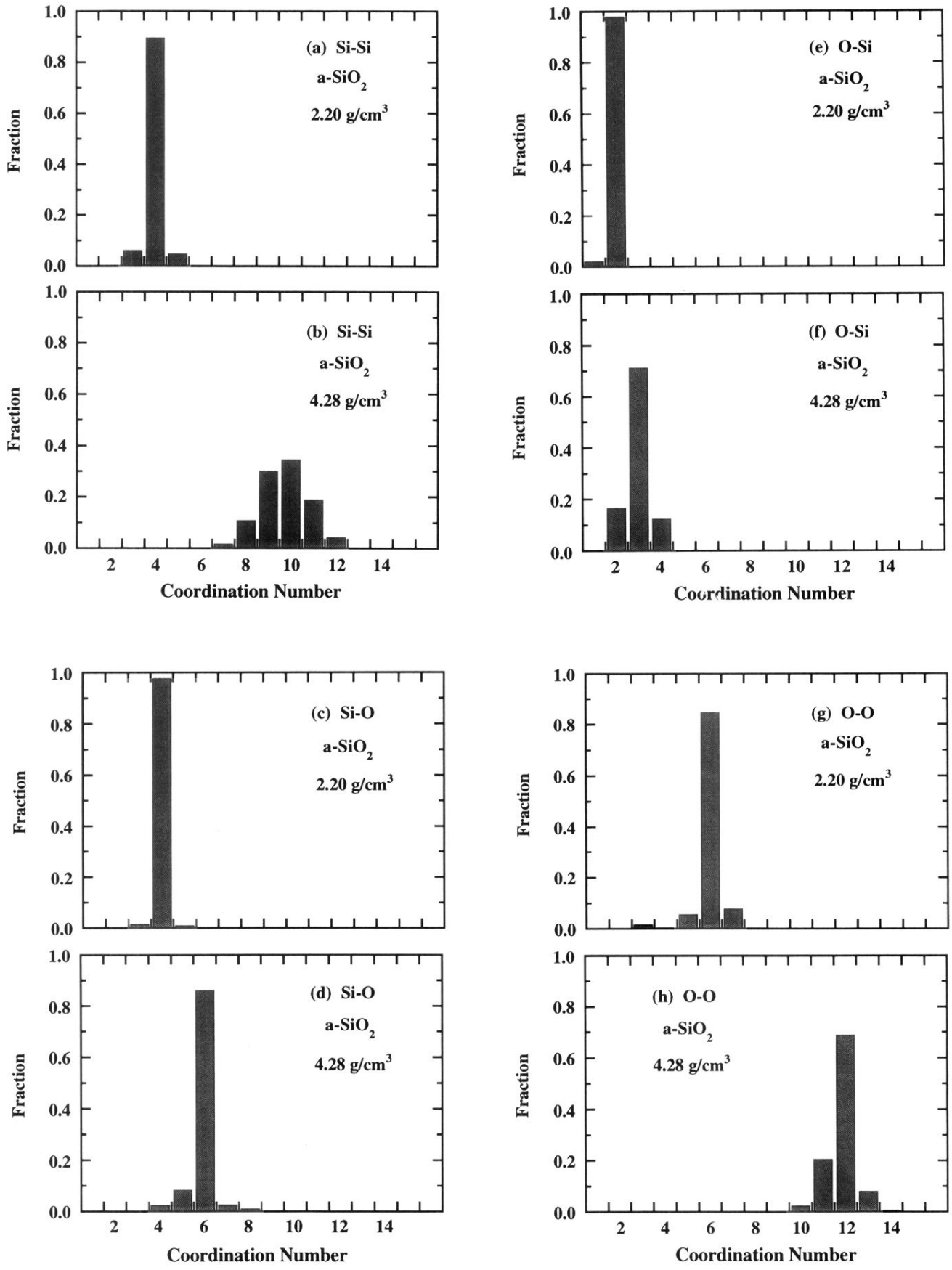

FIG. 2. Distributions of Si and O nearest-neighbor coordinations in SiO_2 glass at 2.20 and 4.28 g/cm^3. In the horizontal axis, each cell represents a coordination category. Vertical bars in each cell represent percentages of a particular coordination.

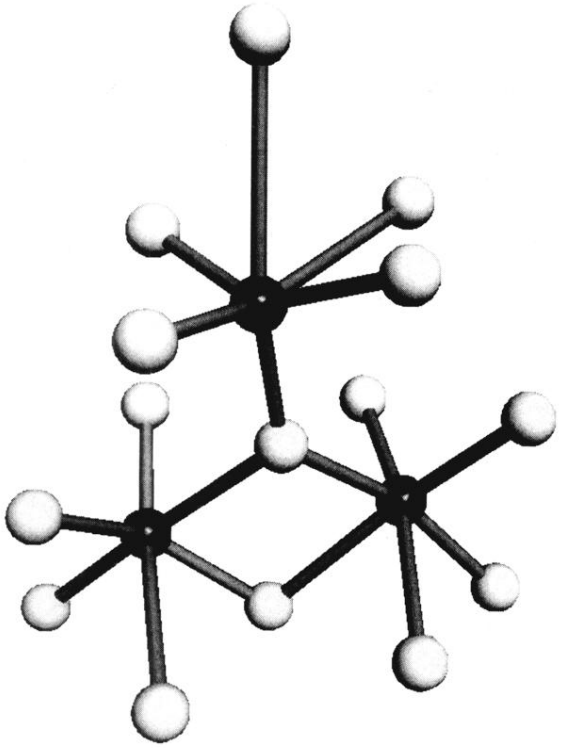

FIG. 5. Arrangement of Si (light spheres) and O (dark spheres) atoms in three Si $(O_{1/3})_6$ octahedra taken from an instantaneous configuration of the highest-density (4.28 g/cm^3) SiO_2 glass obtained in our MD simulation. The bonds connect nearest-neighbor Si-O atoms. The lower two $Si(O_{1/3})_6$ octahedra share one common O-O edge. The upper octahedron shares one common vortex O atom with the lower two octahedra.